




Article

Visible-Light-Driven Antimicrobial Activity and Mechanism of Polydopamine-Reduced Graphene Oxide/BiVO₄ Composite

Biyun Li, Xiaoxiao Gao, Jiangang Qu, Feng Xiong, Hongyun Xuan, Yan Jin * and Huihua Yuan * 

School of Life Sciences, Nantong University, Nantong 226019, China; libiyun1986@163.com (B.L.); g13160495899@163.com (X.G.); qujiangang@ntu.edu.cn (J.Q.); xiongfengxl@163.com (F.X.); hyxuan_seu@163.com (H.X.)

* Correspondence: yjin224@ntu.edu.cn (Y.J.); yuanhh@ntu.edu.cn (H.Y.)

Abstract: In this study, a photocatalytic antibacterial composite of polydopamine-reduced graphene oxide (PDA-rGO)/BiVO₄ is prepared by a hydrothermal self-polymerization reduction method. Its morphology and physicochemical properties are characterized by scanning electron microscopy (SEM), energy-dispersive X-ray spectroscopy (EDX), Fourier-transform infrared (FT-IR), and X-ray diffraction (XRD). The results indicate that BiVO₄ particles are evenly distributed on the rGO surface. *Escherichia coli* (*E. coli*) MG1655 is selected as the model bacteria, and its antibacterial performance is tested by flat colony counting and the MTT method under light irradiation. PDA-rGO/BiVO₄ inhibits the growth of *E. coli* under both light and dark conditions, and light significantly enhances the bacteriostasis of PDA-rGO/BiVO₄. A combination of BiVO₄ with PDA-rGO is confirmed by the above characterization methods as improving the photothermal performance under visible light irradiation. The composite possesses enhanced photocatalytic antibacterial activity. Additionally, the photocatalytic antibacterial mechanism is investigated via the morphology changes in the SEM images of MG1655 bacteria, 2',7'-dichlorofluorescein diacetate (DCFH-DA), the fluorescence detection of the reactive oxygen species (ROS), and gene expression. These results show that PDA-rGO/BiVO₄ can produce more ROS and lead to bacterial death. Subsequently, the q-PCR results show that the transmembrane transport of bacteria is blocked and the respiratory chain is inhibited. This study may provide an important strategy for expanding the application of BiVO₄ in biomedicine and studying the photocatalytic antibacterial mechanism.

Keywords: PDA-rGO/BiVO₄; nanocomposite; antibacterial; mechanism



Citation: Li, B.; Gao, X.; Qu, J.; Xiong, F.; Xuan, H.; Jin, Y.; Yuan, H. Visible-Light-Driven Antimicrobial Activity and Mechanism of Polydopamine-Reduced Graphene Oxide/BiVO₄ Composite. *Int. J. Mol. Sci.* **2022**, *23*, 7712. <https://doi.org/10.3390/ijms23147712>

Academic Editor: Thaqif El Khassawna

Received: 13 June 2022

Accepted: 11 July 2022

Published: 12 July 2022

Publisher's Note: MDPI stays neutral with regard to jurisdictional claims in published maps and institutional affiliations.



Copyright: © 2022 by the authors. Licensee MDPI, Basel, Switzerland. This article is an open access article distributed under the terms and conditions of the Creative Commons Attribution (CC BY) license (<https://creativecommons.org/licenses/by/4.0/>).

1. Introduction

Currently, a variety of pathogenic bacteria seriously threaten human health, which is becoming a major concern for society [1]. There is a growing demand for effective and green environmental antibacterial materials. Photocatalytic materials have attracted widespread attention for the photocatalytic inactivation of bacteria in the field of biomedical applications [2].

BiVO₄ is a kind of visible light photocatalyst that has the advantages of low bandgap energy, green environmental protection, low cost, high stability, and antibacterial activity [3,4]. However, there are some shortcomings of BiVO₄, such as narrow band gap, poor adsorption capacity, and fast electron hole recombination rate [5]. In order to overcome the above issues, researchers have focused on the modification of BiVO₄ with other materials [6–12]. Graphene-based nanomaterials, including graphene oxide (GO) and reduced graphene oxide (rGO), have been proved to have high antibacterial activity [13,14]. They have also been combined with BiVO₄ to inhibit the recombination of electron-hole pairs and improve photocatalytic antibacterial activity by a synergetic effect [15–19]. El-Yazeed et al. [16] added GO to BiVO₄, calcined it at 250 °C, and evaluated the antibacterial behavior against *Escherichia coli* (*E. coli*), *Bacillus subtilis*, and *Candida Albicans*. Pure

BiVO_4 showed little inhibitory activity (<50%) and the antibacterial activity of rGO/ BiVO_4 nanocomposites in the three strains was significantly improved. The synergy between the graphene sheets and BiVO_4 particles plays an important role in enhancing antibacterial activity. However, the above synthesis methods for rGO/ BiVO_4 composites consume a lot of energy. Liao et al. [20] reduced GO with dopamine (DA) and then synthesized Ag-PDA-RGO nanocomposites in situ by adding AgNO_3 . The inhibition rates of GO, PDA-RGO, and Ag-PDA-RGO on *E. coli* were compared. Compared with GO and PDA-RGO, the antibacterial activity of Ag-PDA-RGO nanocomposites was significantly improved, and the antibacterial rate of *E. coli* reached 90.9%. Combining Ag with PDA-rGO significantly improved the antibacterial activity of nanocomposites. DA has recently been used as a green reducing agent for GO [21] and an adhesive agent for BiVO_4 [22]. Nevertheless, BiVO_4 modified with polydopamine-reduced graphene oxide (PDA-rGO) has rarely been reported to have antibacterial applications under visible light irradiation. Additionally, the antibacterial mechanism is not clear.

Hence, in this study, we prepare a photocatalyst of PDA-rGO / BiVO_4 by a hydrothermal self-polymerization reduction method. The photocatalytic antibacterial activity of the synthesized composite is investigated against *E. coli* MG1655. The photocatalytic antibacterial mechanisms determined by bacterial morphological changes, the fluorescence detection of reactive oxygen species (ROS), and gene expression, are discussed.

2. Results and Discussion

2.1. PDA-rGO/ BiVO_4

The as-synthesized BiVO_4 nanoparticles and PDA-rGO/ BiVO_4 composites were examined for morphology and purity by a scanning electron microscope (SEM) equipped with energy-dispersive X-ray spectroscopy (EDX) techniques, as shown in Figure 1A–D. For both pure BiVO_4 and the PDA-rGO/ BiVO_4 composites, the BiVO_4 particles exhibited well-fined flower-like 3D superstructures. The whole flower possessed a 3D eight-pot-shaped structure with high symmetry, which is consistent with previous reports [23,24]. EDX spectra showed the existence of Bi, V, O, and C elements, implying the purity of the samples, as shown in Figure 1C,D. Figure 1E shows the Fourier-transform infrared (FT-IR) spectra of BiVO_4 , PDA-rGO, and PDA-rGO/ BiVO_4 . Both the PDA-rGO and the PDA-rGO/ BiVO_4 FT-IR spectra displayed vibration bands at 1720 cm^{-1} , corresponding to C=O stretching vibrations [21,25]. The peaks at 720 cm^{-1} in both the BiVO_4 and the PDA-rGO/ BiVO_4 composites corresponded to the asymmetric stretching vibration of metal-oxides due to the V-O group, and the shoulder peak at 673 cm^{-1} resulted from the shorter V-O bond, which might be due to the presence of both tetragonal and monoclinic phase structures. The reduction in the distinctive peak at 720 cm^{-1} clearly suggests the presence of a longer asymmetric V-O bond of the pure monoclinic phase [26,27], and these results are consistent with the morphology of BiVO_4 and PDA-rGO/ BiVO_4 (Figure 1A,B). X-ray diffraction (XRD) patterns of the prepared BiVO_4 nanoparticles and the PDA-rGO/ BiVO_4 composite are presented in Figure 1F. The diffraction pattern of BiVO_4 and the PDA-rGO/ BiVO_4 nanocomposite clearly showed sharp peaks in the monoclinic scheelite -phase BiVO_4 [24]. The presence of monoclinic scheelite -phase BiVO_4 in the nanocomposite was confirmed by the (040) plane at 30.5° and the diffraction pattern was in accordance with the JCPDS card number (14-0688) of BiVO_4 [24,26]. Furthermore, the BiVO_4 peak intensity significantly increased with the addition of PDA-rGO to the composite of PDA-rGO/ BiVO_4 . These results suggest that the crystalline nature of BiVO_4 does not change due to the preparation of PDA-rGO and also clearly demonstrates that the BiVO_4 nanosheets were successfully added into the PDA-rGO.

Thus, pure BiVO_4 has certain inhibitory activity, and the antibacterial activity of PDA-rGO/ BiVO_4 nanocomposites is superior to that of pure BiVO_4 , which is consistent with previous studies [16,30]. The structure and morphology of the samples, including surface roughness, surface area, edge sharpness, sheet size, hydrophilicity, dispersion, and functionalization, may control the antibacterial properties of graphene-based nanocomposites [31–33]. Liao et al. [20] compared the inhibition rates of GO, PDA-RGO, and Ag-PDA-RGO on *E. coli*. The antibacterial activity of Ag-PDA-RGO nanocomposites was significantly higher than that of GO and PDA-RGO. The combination of Ag with PDA-rGO significantly improved the antibacterial activity of the nanocomposites. Therefore, the synergistic effect between the PDA-rGO and BiVO_4 particles enhanced the antibacterial activity [16,30].

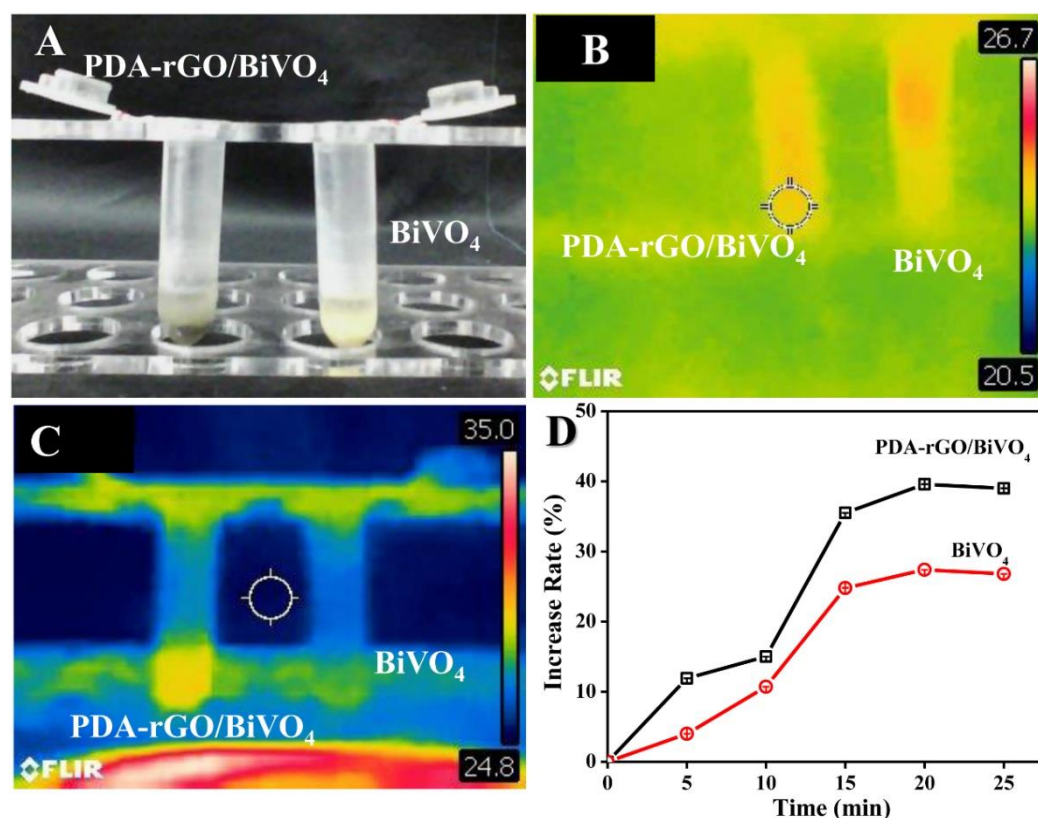


Figure 2. (A) Photograph and (B) infrared thermal images of the BiVO_4 and PDA-rGO/ BiVO_4 composite dispersed in double-distilled water before xenon lamp exposure. (C) Infrared thermal images of the rGO/ BiVO_4 composite after xenon lamp exposure for 10 min. (D) Measured temperature of the composite calculated from infrared thermal images. The symbols are increase rates of BiVO_4 and PDA-rGO/ BiVO_4 .

2.4. ROS Production

It is well-known that the existence of ROS can destroy the stable state of and cause oxidative damage to bacterial cells, ultimately leading to bacterial death [34]. Thus, a 2',7'-dichlorofluorescein diacetate (DCFH-DA) fluorescence method was used to determine ROS production. Under light conditions, the normalized result of the ROS regeneration of individual bacteria treated with PDA-rGO/ BiVO_4 was significantly higher than those treated with BiVO_4 and the control. When treated with BiVO_4 , it was only slightly higher than in the control. On the other hand, under dark conditions, the normalized result of the ROS regeneration of individual bacteria treated with BiVO_4 was comparable to that of the control, but higher than that treated with PDA-rGO/ BiVO_4 . When comparing light and dark conditions, the normalized result of the ROS regeneration of individual bacteria treated with PDA-rGO/ BiVO_4 was significantly higher under light conditions. When treated with

BiVO₄, and in the control group, ROS regeneration was significantly lower under light conditions than under dark conditions (Figure 4). Therefore, a greater generation of ROS is considered as the main reason for the enhanced antibacterial properties of the PDA-rGO/BiVO₄ composite under light irradiation. This is in agreement with previous studies, which showed that modified BiVO₄ can produce more ROS with high oxidation capacity, which is beneficial to the improvement of photocatalytic activity [35,36].

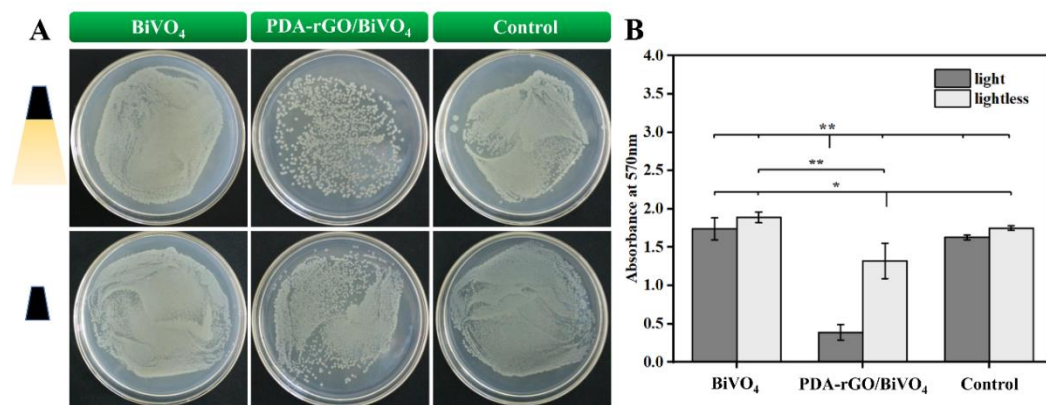


Figure 3. The antibacterial effect of PDA-rGO/BiVO₄ and BiVO₄ with or without xenon light irradiation was determined by flat colony counting (A) and MTT assay (B) (* $p < 0.05$ and ** $p < 0.01$ indicates significant difference).

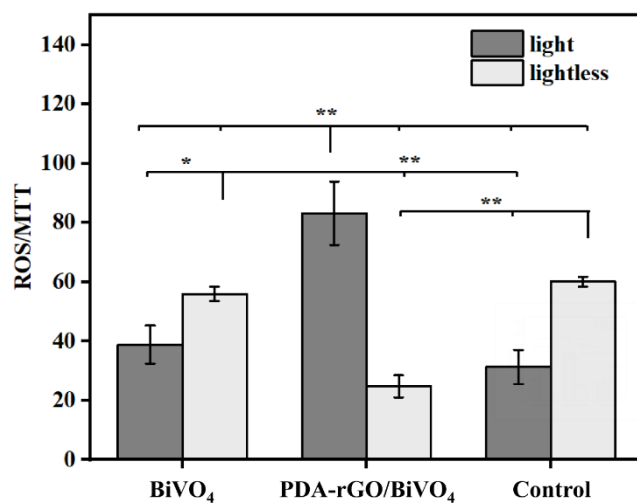


Figure 4. ROS activity normalized to bacteria numbers (* $p < 0.05$ and ** $p < 0.01$ indicate significant difference).

2.5. Microstructures of Bacteria

The morphological changes of *E. coli* before and after treatment with PDA-rGO/BiVO₄ are shown in Figure 5. The survival *E. coli* displayed a short rod-like shape with a complete cell wall [37]. *E. coli* treated with PDA-rGO/BiVO₄ exhibited an irregular ellipsoid shape with incomplete cell structure, indicating bacterial death [38]. Thus, oxidative damage to the cell body with increased ROS resulted in the destruction of the bacterial internal structure. The bacterial cell bodies showed obvious inhibition and adhesion to each other and, finally, the bacterial cell membrane lost its biological function. In conclusion, the ROS produced by PDA-rGO/BiVO₄ under visible light irradiation did some damage to the bacteria. These results further confirm the analysis of antibacterial and ROS fluorescence detection.

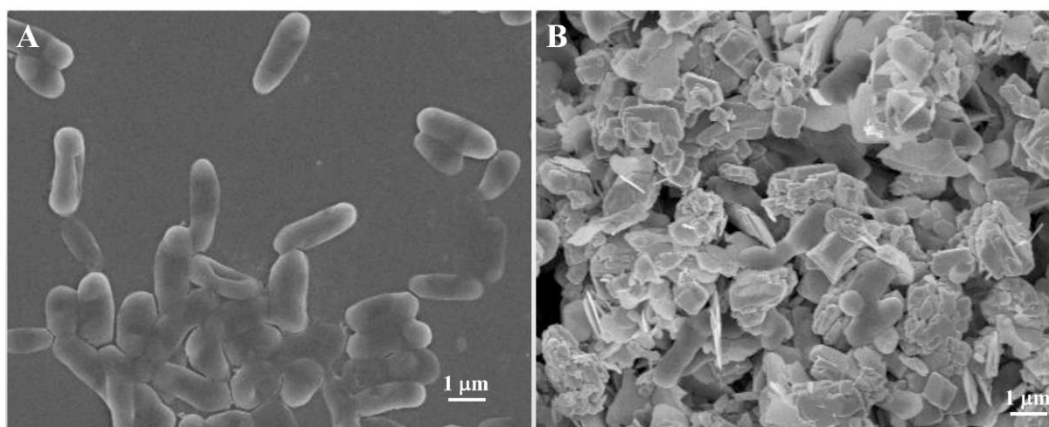


Figure 5. SEM images of *E. coli* (A) and *E. coli* treated with the PDA-rGO/BiVO₄ composite (B).

2.6. Genes Expression

The expression levels of key genes in the PDA-rGO/BiVO₄ treatment group and control group were compared under light conditions. *Thil*, *narU*, and *livK*, encode tRNA uridine 4-sulfurtransferase, nitrate/nitrite transporter, and L-leucine/L-phenylalanine ABC transporter periplasmic-binding protein, respectively, which are involved in the transmembrane transport of substances. Compared with the control group, the expression levels of *thil*, *narU*, and *livK* in the PDA-rGO/BiVO₄ treatment group were down-regulated by 12.99, 13.33, and 3.58 times, respectively (Figure 6). *aceE* encodes the E1 subunit of pyruvate dehydrogenase, which catalyzes the formation of acetyl coenzyme A (CoA) from pyruvate and CoA with the participation of NAD⁺. *PflB* encodes pyruvate lyase, which catalyzes the reaction of acetyl CoA with formic acid to produce CoA and pyruvate. Compared with the control group, the expression level of *aceE* in the PDA-rGO/BiVO₄ treatment group was up-regulated by 2.74 times, while the expression level of *pflB* was slightly decreased. The proteins encoded by *cyoC* and *cyoD* belonged to cytochrome C oxidase (complex IV) in the respiratory chain, and the proteins encoded by *atpC* belonged to ATP synthase (complex V). In the BiVO₄ + rGO treatment group, the expression levels of *cyoC* and *cyoD* were up-regulated by 2.59 times, and the expression levels of *atpC* were down-regulated by 1.85 times.

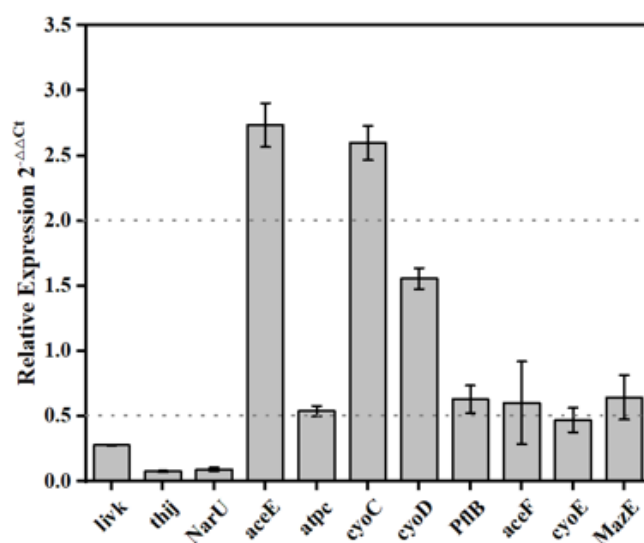


Figure 6. Gene expression of *E. coli* treated with the PDA-rGO/BiVO₄ composite.

Figure 7 exhibits the possible antibacterial mechanisms. The expression levels of *thil*, *narU*, and *livK* genes involved in the transmembrane transport were significantly down-

regulated, which was consistent with a previous study [39]. PDA-rGO/BiVO₄ can produce ROS after photocatalysis, which can lead to the destruction of the phospholipid components of the cell membrane by peroxidation, indicating that photocatalytic disinfection can destroy cell membranes, thus eliminating the transmembrane transport reactions on the cell membrane [40]. The expression level of *aceE* was significantly up-regulated, which was consistent with the results of Liang et al. [39], indicating the increased metabolic flux of CoA. Contrary to the results of Liang et al. [39], the expression level of *pflB* in the catalyzed CoA synthesis reaction was slightly reduced. However, changes in *aceE* and *pflB* can also reduce the content of CoA in cells. Matsunaga et al. found that, in the process of the TiO₂-mediated photochemical sterilization of *E. coli* cells, the content of intracellular CoA decreased, indicating that the photooxidation of CoA is involved in the photocatalytic inactivation of bacteria [41]. Therefore, the photochemical sterilization process mediated by PDA-rGO/BiVO₄ in this study also leads to cell death by reducing the content of CoA in cells. Complex III in the respiratory chain is the main production source of ROS. After PDA-rGO/BiVO₄ photocatalytic treatment, cells produced a large amount of ROS. The up-regulation of *cyoC* and *cyoD* expression in complex IV might be in response to resisting ROS attacks in complex IV. Matsunaga et al. found that cell respiration was inhibited, oxidative phosphorylation was reduced, and ATP synthase was reduced during photocatalytic disinfection [41]. In this study, *atpC* expression level was down-regulated, confirming the inhibition of the respiratory chain.

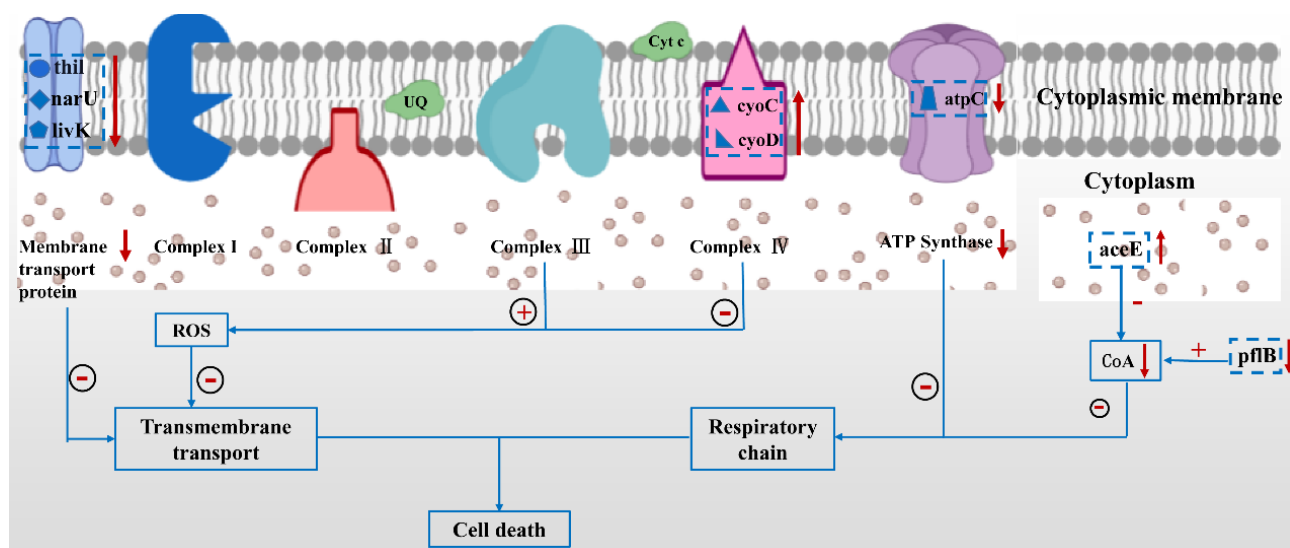


Figure 7. Schematic of the proposed antibacterial mechanism of PDA-rGO/BiVO₄ against *E. coli*. The up/down arrow indicates an increase/decrease in expression, the plus/minus sign indicates a positive/negative effect.

3. Materials and Methods

3.1. Materials

The synthetic precursors used in this preparation were taken as analytical-grade chemicals and subsequently utilized without any further purification. The starting precursors were sodium metavanadate (NaVO₃), bismuth nitrate pentahydrate (Bi(NO₃)₃·5H₂O), ethylenediamine tetraacetic acid disodium salt (EDTA-2Na), HNO₃, and double-distilled (DD) water, which were purchased from Shanghai Chemical Reagent Co., Ltd. (Shanghai, China). GO was obtained from Suzhou Carbon Graphene Technology Co., Ltd. (Suzhou, China). Dopamine hydrochloride was supplied by Bi De Pharmaceutical Technology Co., Ltd. (Shanghai, China). Tris-hydrochloric acid (Tris-HCl) was purchased from Beijing Jingke Hongda Biotechnology Co., Ltd. (Beijing, China).

3.2. Preparation of BiVO_4

The fabrication of BiVO_4 was prepared with reference to our previous work [42]. The synthetic precursor solution, with a pH of 7, contained $\text{Bi}(\text{NO}_3)_3$ (2.911 g), EDTA-2Na (2.500 g), and HNO_3 (10 mL); then, the NaVO_3 (0.732 g) solution was dropped under stirring conditions. The pH value was adjusted to 5 with 1M HNO_3 , then the whole solution was put into a micro reactor and reacted at 160 °C for 1 h under stirring to synthesize the BiVO_4 (Figure 8). Finally, the product was washed with deionized water and dried at 25~30 °C overnight.

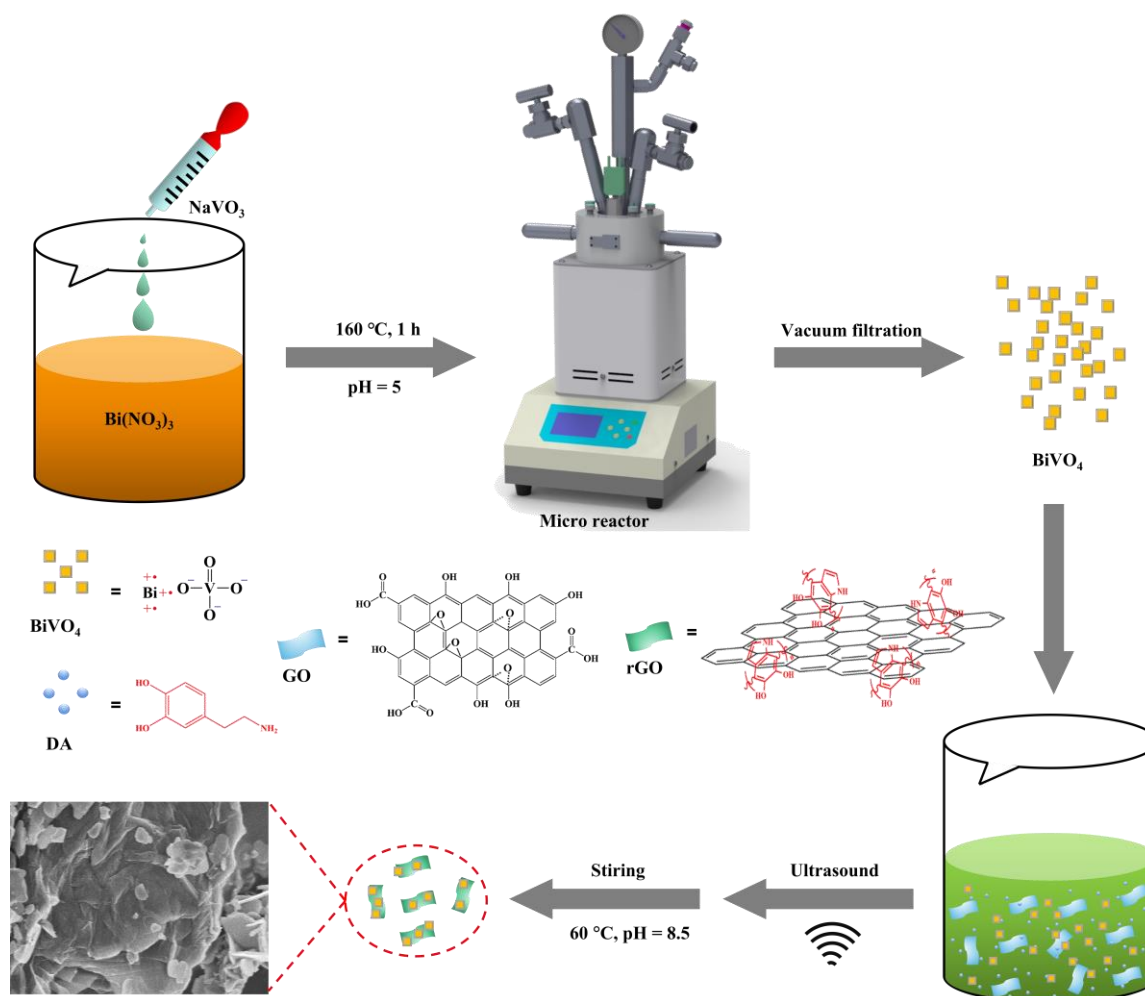


Figure 8. Preparation of PDA-rGO/BiVO_4 nanocomposites.

3.3. PDA-rGO/BiVO_4 Nanocomposite Synthesis

PDA-rGO/BiVO_4 was prepared according to a previously reported synthesis method [21]. Briefly, 50 mg DA, 100 mg GO and already prepared BiVO_4 (100 mg) were added into 200 mL Tris-HCl solution (10 mM, pH = 8.5) and sonicated (150 W) for 15 min in an ice bath. The reaction solution was mechanically stirred for 24 h at 60 °C followed by $3 \times$ centrifugation ($10,000 \times g$) to remove excess polydopamine (PDA). Finally, the products were dried for 24 h at room temperature.

3.4. Characterization

The size and structure of the samples was identified by a field emission scanning electron microscope (FE-SEM, ZEISS Gemini SEM 300, ZEISS, Oberkochen, Germany) within 8–10 kV accelerating voltage. EDX (Aztec X-Max50, Oxford Instruments, Oxford, UK) was used to confirm the elemental composition of the prepared nanocomposites.

The FT-IR spectra of the nanoparticles was carried out on a TENSOR 27 FT-IR spectrometer (Bruker, Munich, Germany) within the range of 600–4000 cm^{-1} at a scanning resolution of 2 cm^{-1} .

XRD (Bruker-AXS APEX2, Germany, analytical $\text{CuK}\alpha$ Rigaku D/max 2550 PC, 40 kV, 300 mA) was used for studying the crystal structure and phase of the sample in the range of 5° to 85° with a 5° (2θ) per min scanning rate.

The visible light photothermal response was acquired by utilizing an infrared thermometer (FLIR C3). Temperatures represent the direct output from the IR system. The temperature of the sample was recorded after being exposed to a 100 W xenon lamp (JY-12610, Jujingyang, Shantou, China) for different time intervals: 0 min, 5 min, 10 min, 15 min, 20 min, and 25 min.

3.5. Antibacterial Ability Assays

E. coli MG1655 (ATCC700926) has been widely used and studied as a model bacterium and has clear genome information. *E. coli* MG1655 was used to assay the antibacterial ability of BiVO_4 and PDA-rGO/ BiVO_4 in this work. *E. coli* was pre-incubated in 5 mL lysogeny broth medium (LB; Feiyu Bio, Nantong, China) at 37 °C and 200 rpm overnight. Then, 10 μL cultures (1×10^5 colony-forming units per milliliter (CFU/mL)) were transferred into the 2 mL microfuge tube containing 400 μL medium. The final concentrations of BiVO_4 and PDA-rGO/ BiVO_4 in the medium were adjusted to 100 mg/mL. LB medium without nano materials was used as the control. Under the condition of open cover, the microfuge tube was irradiated vertically with a xenon lamp for 20 min. Then, *E. coli* was cultured at 37 °C and 200 rpm for 12 h. To ensure the trigger efficiency of light on the nano materials to the bacteria, the same cultures were performed without light. All the tubes were covered with aluminized paper. Cell activity was measured using the MTT assay kit (Beyotime, Shanghai, China). Three independent assays were performed.

LB plate (agar, 15 g/L) was used to show the cell survival ability directly. The treated cells were adjusted to 10^3 diluents. Then, 70 μL diluent was spread evenly on the LB plate and cultured overnight at 37 °C. Three independent assays were performed.

3.6. ROS Analysis

E. coli was cultured in 5 mL LB medium at 37 °C and 200 rpm overnight. One milliliter of the cultures was centrifuged at 4 °C and $8000 \times g$ for 3 min. The pellet was incubated with DCFH-DA, using the ROS Assay Kit (Beyotime, China). Then, 10 μL cells were added into 400 μL LB medium which contained 100 mg/mL BiVO_4 or rGO/ BiVO_4 . LB medium without materials was used as the control. The experiments were conducted both under exposure to a xenon lamp (20 min) and without light. Then, dichlorofluorescein (DCF) fluorescence distribution was detected by fluorospectrophotometer analysis at an excitation wavelength of 488 nm and at an emission wavelength of 525 nm (RF-5301PC, Shimadzu Co. Ltd., Kyoto, Japan). ROS content per MTT unit was calculated to show the ROS amount under the same cell level. Three independent assays were performed.

3.7. Detection of mRNA Levels of Key Genes

E. coli cells treated with PDA-rGO/ BiVO_4 and light were prepared according to “Antibacterial ability assays”. The initial cell concentration was 1×10^6 CFU/mL and the PDA-rGO/ BiVO_4 concentration was 10 mg/mL. The *E. coli* cells cultured with only LB medium and light were used as controls.

One milliliter of the control cultures and two milliliters of the PDA-rGO/ BiVO_4 treated cultures were collected and centrifuged at 4 °C and $10,000 \times g$ for 6 min. After discarding the supernatant, the cells were washed twice with 5 mL sterile ddH_2O . Total RNA was extracted using the TRIzol reagent (Ambion, Austin, TX, USA). The residual DNA was removed and the first-strand cDNA was synthesized in one pot using the Transcript All-in-One First-Strand DNA Synthesis SuperMix for qPCR (One-Step gDNA Removal) Kit (Tsingke, Beijing, China). Quantitative real-time PCR was performed using a set of 2 PCR

primers with SYBR Green I Real-Time PCR (Solarbio, Beijing, China). The PCR analysis was carried out using a 7500 real-time PCR system (Applied Biosystems, Waltham, MA, USA). In all cases, *16S rRNA* was used as a reference gene, and the relative gene expression was calculated by the $2^{-\Delta\Delta CT}$ method. The primers used in this experiment are indicated in Table 1. Five independent assays were performed.

Table 1. Primers used in qRT-PCR.

Gene Name	Description	Forward (5'→3')	Reversed (5'→3')
<i>thiI</i>	tRNA uridine 4-sulfurtransferase	GGCTGTACGTGCTATAAAAG	GCGCAAAAGATGAAAACCAG
<i>narU</i>	nitrate/nitrite transporter	GACATAAACGGAAAGAGCCG	AAAAGCCAAACAAGGGAGCG
<i>aceE</i>	pyruvate dehydrogenase E1 component	CGTCAAGGGCTGGCATAGAT	GGTCGTCTGACTCAGGAGCA
<i>pflB</i>	pyruvate formate-lyase	ATGCTCCCCTGCTCAGGAA	GCTTAATGAAAAGTTAGCCACA
<i>cyoD</i>	cytochrome bo3 ubiquinol oxidase subunit 4	GCAAACAGAAGTGGCAGAT	CTGGCAATGGCAGTGGTACA
<i>cyoC</i>	cytochrome bo3 ubiquinol oxidase subunit 3	CTACCACGTTTAGCGGGCAG	GGCTTCCTGTCAGCGTTCTT
<i>atpC</i>	ATP synthase F1 complex subunit epsilon	GTACCTTCGCTTTGCATTC	TATCTATCTGTCTGGCGGCATT
<i>livK</i>	L-leucine/L-phenylalanine ABC transporter periplasmic binding protein	GTAGGTGCCGTCGGTTCCT	CGTGATTGGGCCGCTGAACT
<i>16S rRNA</i> (reference)	16S ribosomal RNA	CCAACACGGGAAGTCCGCAC	CTGGACGAAGACTGACGCTC

3.8. Statistical Analysis

Statistical analysis of the experimental data was carried out using Origin 8.0 software (OriginLab, Northampton, MA, USA). Variance analysis or the *t*-test were used for comparison between groups. * Indicates a significant difference at $p < 0.05$. ** Indicates a highly significant difference at $p < 0.01$.

4. Conclusions

In summary, PDA-rGO/BiVO₄ hybrid materials were successfully prepared by a hydrothermal self-polymerization reduction method and BiVO₄ particles were evenly distributed on the rGO surface. The combination of PDA-rGO and BiVO₄ effectively improved the utilization of the visible-light-driven thermal effect. The photocatalytic inactivation of *E. coli* with the synthetic PDA-rGO/BiVO₄ was superior to that of pure BiVO₄ under visible light irradiation. The DCFH-DA fluorescence method was used to determine the production of ROS. Under light conditions, PDA-rGO/BiVO₄ produced more ROS with high oxidation capacity, which was beneficial to the improvement of photocatalytic activity. According to the morphology changes in the SEM images of *E. coli* MG1655, *E. coli* treated with PDA-rGO/BiVO₄ exhibited an irregular ellipsoid shape with an incomplete cell structure, indicating bacterial death. Mechanistically, the ROS produced by the PDA-rGO/BiVO₄ penetrated the bacterial cell membrane and caused oxidative damage, blocked the transmembrane transport of bacteria, and inhibited the respiratory chain, which was confirmed by ROS fluorescence detection, morphological changes, and gene expression.

Author Contributions: B.L., methodology, investigations, writing—original draft, writing—review and editing; X.G., methodology, investigation; J.Q., methodology, investigation; F.X., methodology, investigation; H.X., methodology, investigation; Y.J., supervision, data curation, writing—review and

editing; H.Y., supervision, project administration, resources, data curation, visualization, writing—review and editing. All authors have read and agreed to the published version of the manuscript.

Funding: This research was funded by the National Natural Science Foundation of China (81801856 and 32000965), the Natural Science Foundation of Jiangsu Province (BK20200964), the Project of Natural Science Research of Higher Education Institutions of Jiangsu Province (20KJB430042) and Large Instruments Open Foundation of Nantong University.

Institutional Review Board Statement: Not applicable.

Informed Consent Statement: Not applicable.

Data Availability Statement: All relevant data are presented in the manuscript; raw data are available upon request from the corresponding author.

Conflicts of Interest: The authors declare no conflict of interest.

References

1. Chen, Y.F.; Tang, X.N.; Gao, X.; Zhang, B.; Luo, Y.; Yao, X.Y. Antimicrobial property and photocatalytic antibacterial mechanism of the TiO₂-doped SiO₂ hybrid materials under ultraviolet-light irradiation and visible-light irradiation. *Ceram. Int.* **2019**, *45*, 15505–15513. [[CrossRef](#)]
2. Zhang, Q.; Sun, C.; Zhao, Y.; Zhou, S.; Hu, X.; Chen, P. Low Ag-doped titanium dioxide nanosheet films with outstanding antimicrobial property. *Environ. Sci. Technol.* **2010**, *44*, 8270–8275. [[CrossRef](#)] [[PubMed](#)]
3. Thomas, C.T.; Manisekaran, R.; Santoyo-Salazar, J.; Schoefs, B.; Velumani, S.; Castaneda, H.; Jantrania, A. Graphene oxide decorated TiO₂ and BiVO₄ nanocatalysts for enhanced visible-light-driven photocatalytic bacterial inactivation. *J. Photochem. Photobiol. A-Chem.* **2021**, *418*, 113374.
4. Qu, Z.; Liu, P.; Yang, X.; Wang, F.; Zhang, W.; Fei, C. Microstructure and characteristic of BiVO₄ prepared under different pH values: Photocatalytic efficiency and antibacterial activity. *Materials* **2016**, *9*, 129. [[CrossRef](#)] [[PubMed](#)]
5. Guo, J.Y.; Li, X.; Liang, J.; Yuan, X.Z.; Jiang, L.B.; Yu, H.B.; Sun, H.B.; Zhu, Z.Q.; Ye, S.J.; Tang, N.; et al. Fabrication and regulation of vacancy-mediated bismuth oxyhalide towards photocatalytic application: Development status and tendency. *Coord. Chem. Rev.* **2021**, *443*, 214033. [[CrossRef](#)]
6. Yan, Y.; Ni, T.; Du, J.; Li, L.; Fu, S.; Li, K.; Zhou, J. Green synthesis of balsam pear-shaped BiVO₄/BiPO₄ nanocomposite for degradation of organic dye and antibiotic metronidazole. *Dalton Trans.* **2018**, *47*, 6089–6101. [[CrossRef](#)]
7. Jafari, N.; Ebrahimpour, K.; Abdollahnejad, A.; Karimi, M.; Ebrahimi, A. Efficient degradation of microcystin-LR by BiVO₄/TiO₂ photocatalytic nanocomposite under visible light. *J. Environ. Health Sci. Eng.* **2020**, *17*, 1171–1183. [[CrossRef](#)]
8. Trinh, D.T.T.; Channei, D.; Nakaruk, A.; Khanitchaidecha, W. New insight into the photocatalytic degradation of organic pollutant over BiVO₄/SiO₂/GO nanocomposite. *Sci. Rep.* **2021**, *11*, 4620. [[CrossRef](#)]
9. Lee, G.J.; Lee, X.Y.; Lyu, C.; Liu, N.; Andandan, S.; Wu, J.J. Sonochemical synthesis of copper-doped BiVO₄/g-C₃N₄ nanocomposite materials for photocatalytic degradation of bisphenol a under simulated sunlight irradiation. *Nanomaterials* **2020**, *10*, 498. [[CrossRef](#)]
10. Sun, J.; Wang, C.; Shen, T.; Song, H.; Li, D.; Zhao, R.; Wang, X. Engineering the dimensional interface of BiVO₄-2D reduced graphene oxide (RGO) nanocomposite for enhanced visible light photocatalytic performance. *Nanomaterials* **2019**, *9*, 907. [[CrossRef](#)]
11. Wang, Y.; Long, Y.; Zhang, D. Novel bifunctional V₂O₅/BiVO₄ nanocomposite materials with enhanced antibacterial activity. *J. Taiwan Inst. Chem. Eng.* **2016**, *68*, 387–395. [[CrossRef](#)]
12. Tayebi, M.; Tayyebi, A.; Lee, B.K.; Lee, C.H.; Lim, D.H. The effect of silver doping on photoelectrochemical (PEC) properties of bismuth vanadate for hydrogen production. *Sol. Energy Mater. Sol. Cells* **2019**, *200*, 109943. [[CrossRef](#)]
13. Zhao, M.; Shan, T.; Wu, Q.; Gu, L. The antibacterial effect of graphene oxide on *Streptococcus mutans*. *J. Nanosci. Nanotechnol.* **2020**, *20*, 2095–2103. [[CrossRef](#)] [[PubMed](#)]
14. Kumar, P.; Huo, P.; Zhang, R.; Liu, B. Antibacterial properties of graphene-based nanomaterials. *Nanomaterials* **2019**, *9*, 737. [[CrossRef](#)]
15. Sharma, R.; Uma, Singh, S.; Verma, A.; Khanuja, M. Visible light induced bactericidal and photocatalytic activity of hydrothermally synthesized BiVO₄ nano-octahedrals. *J. Photochem. Photobiol. B-Biol.* **2016**, *162*, 266–272. [[CrossRef](#)]
16. El-Yazeed, W.S.A.; El-Hakam, S.A.; Salah, A.A.; Ibrahim, A.A. Fabrication and characterization of reduced graphene-BiVO₄ nanocomposites for enhancing visible light photocatalytic and antibacterial activity. *J. Photochem. Photobiol. A Chem.* **2021**, *417*, 113362. [[CrossRef](#)]
17. Yan, Y.; Sun, S.; Song, Y.; Yan, X.; Guan, W.; Liu, X.; Shi, W. Microwave-assisted in situ synthesis of reduced graphene oxide-BiVO₄ composite photocatalysts and their enhanced photocatalytic performance for the degradation of ciprofloxacin. *J. Hazard. Mater.* **2013**, *250*, 106–114. [[CrossRef](#)]
18. Ng, Y.H.; Iwase, A.; Bell, N.J.; Kudo, A.; Amal, R. Semiconductor/reduced graphene oxide nanocomposites derived from photocatalytic reactions. *Catal. Today* **2011**, *164*, 353–357. [[CrossRef](#)]

19. Fu, Y.; Sun, X.; Wang, X. BiVO₄-graphene catalyst and its high photocatalytic performance under visible light irradiation. *Mater. Chem. Phys.* **2011**, *131*, 325–330. [[CrossRef](#)]
20. Liao, J.; He, S.; Guo, S.; Luan, P.; Mo, L.; Li, J. Antibacterial performance of a mussel-inspired polydopamine-treated Ag/graphene nanocomposite material. *Materials* **2019**, *12*, 3360. [[CrossRef](#)]
21. Li, B.Y.; Xiong, F.; Yao, B.; Du, Q.; Cao, J.; Qu, J.G.; Feng, W.; Yuan, H.H. Preparation and characterization of antibacterial dopamine-functionalized reduced graphene oxide/PLLA composite nanofibers. *RSC Adv.* **2020**, *10*, 18614–18623. [[CrossRef](#)] [[PubMed](#)]
22. Ran, J.; Bi, S.; Jiang, H.; Telegin, F.; Bai, X.; Yang, H.; Cheng, D.; Cai, G.; Wang, X. Core-shell BiVO₄@PDA composite photocatalysts on cotton fabrics for highly efficient photodegradation under visible light. *Cellulose* **2019**, *26*, 6259–6273. [[CrossRef](#)]
23. Ou, M.; Zhong, Q.; Zhang, S.L.; Nie, H.Y.; Lv, Z.J.; Cai, W. Graphene-decorated 3D BiVO₄ superstructure: Highly reactive (040) facets formation and enhanced visible-light-induced photocatalytic oxidation of NO in gas phase. *Appl. Catal. B-Environ.* **2016**, *193*, 160–169. [[CrossRef](#)]
24. Vidya, J.; Bosco, A.J.; Haribaaskar, K.; Balamurugan, P. Polyaniline-BiVO₄ nanocomposite as an efficient adsorbent for the removal of methyl orange from aqueous solution. *Mater. Sci. Semicond. Process* **2019**, *103*, 104645. [[CrossRef](#)]
25. Azad, R.; Bezaatpour, A.; Amiri, M.; Eskandari, H.; Nouhi, S.; Taffa, D.H.; Wark, M.; Boukherroub, R.; Szunerits, S. Excellent photocatalytic reduction of nitroarenes to aminoarenes by BiVO₄ nanoparticles grafted on reduced graphene oxide (rGO/BiVO₄). *Appl. Organomet. Chem.* **2019**, *33*, e5059. [[CrossRef](#)]
26. Packiaraj, R.; Venkatesh, K.S.; Devendran, P.; Bahadur, S.A.; Nallamuthu, N. Structural, morphological and electrochemical studies of nanostructured BiVO₄ for supercapacitor application. *Mater. Sci. Semicond. Process* **2020**, *115*, 105122. [[CrossRef](#)]
27. Zhang, A.P.; Zhang, J.Z. Hydrothermal processing for obtaining of BiVO₄ nanoparticles. *Mater. Lett.* **2009**, *63*, 1939–1942. [[CrossRef](#)]
28. Vasileiadis, T.; Dalvise, T.M.; Saak, C.M.; Pochylski, M.; Harvey, S.; Synatschke, C.V.; Gapinski, J.; Fytas, G.; Backus, E.H.G.; Weil, T.; et al. Fast light-driven motion of polydopamine nanomembranes. *Nano Lett.* **2022**, *22*, 578–585. [[CrossRef](#)]
29. Zong, P.; Liang, J.; Zhang, P.; Wan, C.; Wang, Y.; Koumoto, K. Graphene-based thermoelectrics. *ACS Appl. Energy Mater.* **2020**, *3*, 2224–2239. [[CrossRef](#)]
30. Saleem, A.; Ahmed, T.; Ammar, M.; Zhang, H.L.; Xu, H.B.; Tabassum, R. Direct growth of m-BiVO₄@carbon fibers for highly efficient and recyclable photocatalytic and antibacterial applications. *J. Photochem. Photobiol. B Biol.* **2020**, *213*, 112070. [[CrossRef](#)]
31. Hegab, H.M.; ElMekawy, A.; Zou, L.; Mulcahy, D.; Saint, C.P.; Ginic-Markovic, M. The controversial antibacterial activity of graphene-based materials. *Carbon* **2016**, *105*, 362–376. [[CrossRef](#)]
32. Jeevitha, G.; Abhinayaa, R.; Mangalaraj, D.; Ponpandian, N. Tungsten oxide-graphene oxide (WO₃-GO) nanocomposite as an efficient photocatalyst, antibacterial and anticancer agent. *J. Phys. Chem. Solids* **2018**, *116*, 137–147. [[CrossRef](#)]
33. Jovanovic, S.; Holclajtner-Antunovic, I.; Uskokovic-Markovic, S.; Bajuk-Bogdanovic, D.; Pavlovic, V.; Tosic, D.; Milenkovic, M.; Markovic, B.T. Modification of graphene oxide surfaces with 12-molybdophosphoric acid: Structural and antibacterial study. *Mater. Chem. Phys.* **2018**, *213*, 157–167. [[CrossRef](#)]
34. Aditya, A.; Chattopadhyay, S.; Jha, D.; Gautam, H.K.; Maiti, S.; Ganguli, M. Zinc oxide nanoparticles dispersed in ionic liquids show high antimicrobial efficacy to skin-specific bacteria. *ACS Appl. Mater. Interfaces* **2018**, *10*, 15401–15411. [[CrossRef](#)] [[PubMed](#)]
35. Phanichphant, S.; Nakaruk, A.; Chansaenpak, K.; Channei, D. Evaluating the photocatalytic efficiency of the BiVO₄/rGO photocatalyst. *Sci. Rep.* **2019**, *9*, 16091. [[CrossRef](#)]
36. Jin, Z.; Zhang, Y.; Liu, D.; Ding, H.; Mamba, B.B.; Kuvarega, A.T.; Gui, J. Fabrication of a La-doped BiVO₄@CN step-scheme heterojunction for effective tetracycline degradation with dual-enhanced molecular oxygen activation. *Sep. Purif. Technol.* **2021**, *277*, 119224. [[CrossRef](#)]
37. Wu, W.; Zhao, W.; Wu, Y.; Zhou, C.; Li, L.; Liu, Z.; Dong, J.; Zhou, K. Antibacterial behaviors of Cu₂O particles with controllable morphologies in acrylic coatings. *Appl. Surf. Sci.* **2019**, *465*, 279–287. [[CrossRef](#)]
38. Cai, Q.; Gao, Y.; Gao, T.; Lan, S.; Simalou, O.; Zhou, X.; Zhang, Y.; Harnooode, C.; Gao, G.; Dong, A. Insight into biological effects of zinc oxide nanoflowers on bacteria: Why morphology matters. *ACS Appl. Mater. Interfaces* **2016**, *8*, 10109–10120. [[CrossRef](#)]
39. Liang, X.L.; Liang, Z.M.; Wang, S.; Chen, X.H.; Ruan, Y.; Zhang, Q.Y.; Zhang, H.Y. An analysis of the mechanism underlying photocatalytic disinfection based on integrated metabolic networks and transcriptional data. *J. Environ. Sci.* **2020**, *92*, 28–37. [[CrossRef](#)]
40. Zhang, J.; Wang, X.; Suo, X.; Liu, X.; Liu, B.; Yuan, M.; Wang, G.; Liang, C.; Shi, H. Cellular response of *Escherichia coli* to photocatalysis: Flagellar assembly variation and beyond. *ACS Nano* **2019**, *13*, 2004–2014.
41. Matsunaga, T.; Tomoda, R.; Nakajima, T.; Wake, H. Photoelectrochemical sterilization of microbial cells by semiconductor powders. *FEMS Microbiol. Lett.* **1985**, *29*, 211–214. [[CrossRef](#)]
42. Qu, J.G.; Qian, J.Q.; Wu, M.T.; Mao, Q.H.; Li, M. Hydrothermal synthesis of cotton-based BiVO₄/Ag composite for photocatalytic degradation of CI Reactive Black 5. *RSC Adv.* **2020**, *10*, 39295–39303. [[CrossRef](#)] [[PubMed](#)]